Mechanical characterization and modeling of knitted textile implants with permanent set

Baptiste Pierrat, Vít Nováček, Stéphane Avril, Frédéric Turquier

Mechanical characterization and modeling of knitted textile implants with permanent set

B. Pierrat[a,*], Vít Nováček[b], S. Avril[a], F. Turquier[a]

[a] *Mines Saint-Etienne, Univ Lyon, Univ Jean Monnet, INSERM, U 1059 Sainbiose, Centre CIS, F - 42023 Saint-Etienne France*
[b] *New Technologies — Research Centre, University of West Bohemia, Univerzitní 8, 301 00 Plzeň, Czech Republic*

Abstract

Textile-based implant (mesh) treatment is considered as a standard of care for abdominal wall hernia repair. Computational models and simulations have appeared as one of the most promising approach to investigate biomechanics related to hernia repair and to improve clinical outcomes. This paper presents a novel anisotropic hypo-elastoplastic constitutive model specifically established for surgical knitted textile implants. The major mechanical characteristics of these materials such as anisotropy and permanent set have been reproduced. For the first time ever, we report an extensive mechanical characterization of one of these meshes, including cyclic uniaxial tension, planar equibiaxial tension and plunger type testing. These tests highlight the complex mechanical behavior with strong nonlinearity, anisotropy and permanent set. The novel anisotropic hypo-elasto-plastic constitutive model has been identified based on the tensile experiments and validated successfully against the data of the plunger experiment. In the future, implementation of this characterization and modeling approach to additional surgical knitted textiles should be the direction to follow in order to develop clinical decision support software for abdominal wall repair.

Keywords: abdominal wall hernia, knitted textile-based implant, constitutive modeling

*Corresponding author
Email address: pierrat@emse.fr (B. Pierrat)

1. Introduction

Ventral incisional hernia (VIH) is the protrusion of abdomen contents through a weakness of the abdominal wall at an incision closure site. VIH repair is one of the most common surgical procedures worldwide. Despite the general use of textile based implants over the past two decades, complications have remained very high. Recurrence rates have been reported close to 11% and over 44% respectively for general and high risk patient populations [4, 3]. The average hospital costs associated with ventral and incisional hernia repair for a patient have been estimated to 10 700$ in the US [23] and 6 451€ in France [12]. This should be put in perspective with the very high number of interventions, around 350 000 annually in the US [27] and 65 000 in France [12]. The absence of consensus has led to tremendous variation in treatment outcomes, costs and resource utilization. Moreover, VIH repair suffers drastically from a lack of treatment personalization. Numerical modeling and simulation have appeared as one of the most promising approach to investigate biomechanics related to VIH repair, to identify influential parameters, to optimize and customize textile implants in combination with surgical techniques, and finally, to improve clinical outcomes.

Surgical textiles are highly conformable and porous structures that result from the knitting of fibers. Their mechanical behavior and strength depend upon the fiber diameter, the material composition, the effect of the manufacturing process, the knitting patterns, the shapes and dimensions, and finally upon the loading conditions. Surgical textiles exhibit an anisotropic non-linear behavior with high (nonlinear) Poisson's ratio. Hysteresis is also commonly observed when submitting these textiles to uniaxial and planar biaxial tensile loads [8, 7, 6, 11].

Computational simulations of such complex behavior have been attempted at the fiber scale [10, 18, 20, 9]. These models have revealed a very high potential as they can take into account the impact of the knitting process on the fibers (geometry and material properties), deal with fiber-fiber interactions and open the way for multi-scale modeling (micro/meso/macro). However, due to

prohibitive computational costs, only the standard Jersey fabric has been considered so far. This simple pattern is too far apart from the ones of regular surgical textiles used in VIH repair.

Numerous homogenized models have also been developed at the macroscopic scale. Textiles are then assumed as homogenous and continuous media and modeled using the theory of hyperelasticity [31, 13, 21]. Their constitutive equations derive from strain energy functions developed initially for biological [14] or rubber-like soft tissues [1]. Although anisotropic, their characterization remains exclusively based on monotonous uniaxial tensile tests. Therefore, there is an urgent need to carry out multi-axial cyclic tests reproducing physiological loading conditions in order to calibrate computational models.

In this study, advanced uni-axial and multi-axial experiments were conducted to identify and validate a novel anisotropic hypo-elastoplastic constitutive model specifically established for surgical knitted textile implants, including all the major mechanical characteristics of these materials such as anisotropy and permanent set.

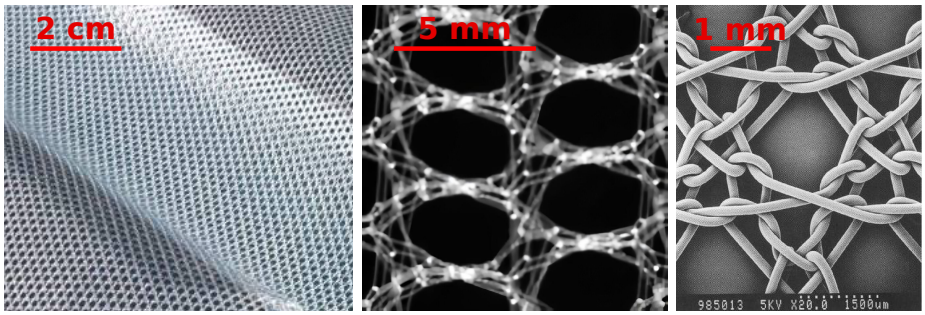

Figure 1: Illustration of the different scales and complex structure of knitted hernia meshes.

2. Materials and Methods

2.1. Constitutive modelling

Surgical knitted textiles were modeled using the membrane theory for very thin shells, neglecting bending and twisting moments. A bi-dimensional plane

stress formulation was adopted, relating the vector made of the 3 in-plane components of the logarithmic strain tensor $\{\boldsymbol{\varepsilon}\} = \{\varepsilon_{11}; \varepsilon_{22}; \varepsilon_{12}\}$ to the vector made of the 3 in-plane components of the Cauchy stress tensor $\{\boldsymbol{\sigma}\} = \{\sigma_{11}; \sigma_{22}; \sigma_{12}\}$, where directions 1 and 2 are the local warp and weft directions of the knitted textile respectively.

Anisotropy, non-linearity and permanent set of the surgical knitted textiles were captured with an original anisotropic hypo-elastoplastic membrane model. The constitutive model was based on an additive split of the logarithmic strain tensor into a plastic strain $\{\boldsymbol{\varepsilon^{pl}}\}$ representing the permanent set of the mesh, and an elastic strain $\{\boldsymbol{\varepsilon^{el}}\}$ such as $\{\boldsymbol{\varepsilon}\} = \{\boldsymbol{\varepsilon^{el}}\} + \{\boldsymbol{\varepsilon^{pl}}\}$.

The stress rate is obtained using an incremental formulation such as:

$$\{\overset{\square}{\boldsymbol{\sigma}}\} = [\boldsymbol{C}(\boldsymbol{\varepsilon}^{el})]\{\dot{\boldsymbol{\varepsilon}}^{\boldsymbol{el}}\} = g(\boldsymbol{\varepsilon})[\boldsymbol{C}(\boldsymbol{\varepsilon}^{el})]\{\dot{\boldsymbol{\varepsilon}}\} \tag{1}$$

where $\{\dot{\boldsymbol{\varepsilon}}^{\boldsymbol{el}}\}$ is the elastic strain rate, $\{\dot{\boldsymbol{\varepsilon}}\}$ is the total strain rate, $\{\overset{\square}{\boldsymbol{\sigma}}\} = \{\dot{\boldsymbol{\sigma}}\} + \{\Omega.\boldsymbol{\sigma}\} - \{\boldsymbol{\sigma}.\Omega\}$ is the Green-Naghdi rate of the Cauchy stress and Ω is the spin tensor.

Despite the anisotropy of the surgical textiles, it is assumed (assumption verified in the Results section, see Fig. 2) that there exists a unique scalar function $f(\varepsilon_{ij}) = \frac{a(\varepsilon_{ij})^2}{(\varepsilon_{ij})^2 + b\varepsilon_{ij} + c}$ such as $\varepsilon_{ij}^{el} = f(\varepsilon_{ij})$ and:

$$g(\varepsilon_{ij}) = \frac{\partial f}{\partial \varepsilon_{ij}} = \frac{\dot{\varepsilon}_{ij}^{el}}{\dot{\varepsilon}_{ij}} \tag{2}$$

$[\boldsymbol{C}(\boldsymbol{\varepsilon}^{el})]$ is the strain-dependent tangent stiffness matrix which may be written for a membrane such as:

$$[\boldsymbol{C}(\boldsymbol{\varepsilon}^{el})] = \begin{bmatrix} \frac{1}{E_1^0 + E_1^1 \varepsilon_{11}^{el}} & -\frac{\nu_{12}}{E_1^0 + E_1^1 \varepsilon_{11}^{el}} & 0 \\ -\frac{\nu_{12}}{E_1^0 + E_1^1 \varepsilon_{11}^{el}} & \frac{1}{E_2^0 + E_2^1 \varepsilon_{221}^{el}} & 0 \\ 0 & 0 & \frac{1}{G_{12}^0 + G_{12}^1 \varepsilon_{12}^{el}} \end{bmatrix}^{-1} \tag{3}$$

Eventually, there are 10 parameters to identify in the constitutive model:

- The 6 stiffness constants E_1^0, E_1^1, E_2^0, E_2^1, G_{12}^0 and G_{12}^1,
- the Poisson's ratio ν_{12},

- the 3 parameters of the yield evolution function a, b and c.

The methodology used to identify these parameters is described in Section 2.3.

2.2. Mechanical characterization

Uniaxial and equibiaxial quasi-static cyclic tests were carried out in a 37°C water bath, on specimens presenting a gauge area of 25x25 mm^2. Uniaxial quasi-static cyclic tests were carried out with an Instron© ElectroPuls E3000 system fitted with a 250 N load cell. Tension was applied in 3 different directions of the textile: warp, weft and diagonal (45°). The machine was controlled in displacement with a jaw velocity of 0.25 mm/s. Cyclic displacement ramps were performed. Each stage consisted of 5 cycles, with a loading reaching x% maximum strain and an unloading to 0 N. The maximum strain applied at each stage x was successively increased, taking the following values: 5%, 10%, 15%, 20%, 25%.

A TA Instruments ElectroForce® planar biaxial test machine was used to carry out the equibiaxial tensile tests and assess the mechanical coupling between warp and weft directions. The force was measured in each direction with two 225 N load cells and the machine being controlled in load. Ten cycles were applied between 0 and 40 N on each sample, inducing a tension of 16 N/cm similar to the effects of intra-abdominal pressure loading reported by Klinge et al. [17].

For both uniaxial and biaxial tensile tests, logarithmic strains were assessed from the length separating the holding jaws $\varepsilon = \log(\frac{L}{L_0})$ where L was the current length and L_0 the initial length.

The Cauchy stress values were calculated assuming a thickness t of 0.5 mm. Note that this thickness is an average value at the macroscopic scale where the textile is modelled as a continuum medium. The Cauchy stress was derived as $\sigma = \frac{F}{t\,w}$ where F is the measured load and w is the current width measured using a camera and the VIC-3D^{TM} (Correlated Solutions) digital image correlation system.

2.3. Identification technique

After performing the experiments, the obtained experimental stress-strain curves (see Figure 4) were separated into two regions for post-processing:

- the envelope, *i.e.* the part when the plastic strain increases with the load,
- the cycles, *i.e.* the unloading and reloading part obtained after the first loading of each stage. During the cycles, the plastic strain remains constant.

2.3.1. Tangent moduli in warp and weft directions

The unloading and reloading stage of the last cycle was extracted and averaged (neglecting hysteresis effects) for the warp and weft directions in the uniaxial tensile tests. It is assumed that during this stage the response is purely elastic (Figure 5a). A 2^{nd} order polynomial function was fitted to these elastic stress-strain curves with a least-squares algorithm implemented in Matlab® (Figure 5a), yielding the 4 stiffness constants E_1^0, E_1^1, E_2^0 and E_2^1.

2.3.2. Yield evolution function

Under uniaxial tension, the accumulated permanent strain after unloading depended on the maximum strain value which was previously reached. The evolution law was similar regardless of the loading direction (Figure 2). This evolution was determined by plotting the elastic strain as a function of total strain for the envelope, using the previously determined elastic stress-strain response: at a given σ, (i) the elastic strain was determined from Figure 5a and (ii) the total strain was determined from the envelope. Then, the elastic strain was plotted against the total strain for warp and weft directions, again showing an isotropic behavior in this response. A 2^{nd} order rational polynomial was used to fit these data points with a least-square algorithm in Matlab® (Figure 5b), yielding constitutive parameters a, b and c.

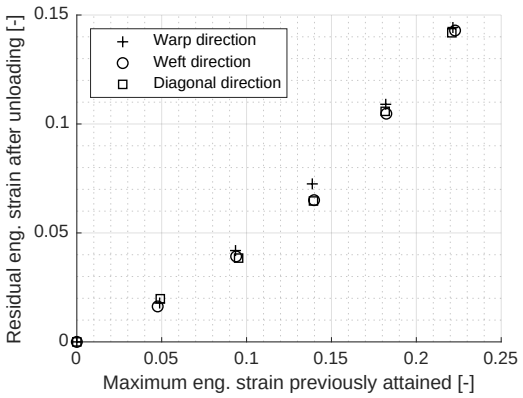

Figure 2: Permanent set evolution for uniaxial tensile tests as a function of maximum applied strain. The permanent set was derived as the residual strain obtained after unloading. The curves show that the evolution of the permanent set is similar in the warp, weft and diagonal directions.

2.3.3. Poisson's ratio

Equibiaxial stress-strain curves were used to identify the Poisson's ratio ν_{12}, after identifying the 4 stiffness constants E_1^0, E_1^1, E_2^0 and E_2^1. A linear least-square fitting was used to determine ν_{12} from the stress-strain response curves of equibiaxial experiments (Figure 4d). Note that uniaxial experiments were not used for this identification; the free boundary conditions on the edges made the textile curl slightly, over-estimating the effective lateral contraction.

2.3.4. Shear modulus

The diagonal tensile experiments could not be used directly for identifying G_{12}^0 and G_{12}^1, as this experiment involves a mix of tension and shear. Another issue with this experiment is that it is not statically determined for finite deformations (there is no analytical expression of the local stress as a function of the applied load). Consequently, an inverse problem must be formulated and solved. A single finite-element was coded in Matlab® with the previously identified constitutive parameters, and submitted to the diagonal tensile test. At every strain increment, the tangent modulus $G_{12}(\varepsilon_{12}^{el})$ was identified to fit the

diagonal stress-strain response. Then, this function was approximated with a linear function to derive G_{12}^0 and G_{12}^1.

2.4. Abaqus implementation

The models were implemented and solved using the commercial finite-element (FE) software Abaqus®/Explicit.

The constitutive behaviour relating the strain rates to the Cauchy stress rates is the core of the explicit solver and was implemented as a VUMAT subroutine in Abaqus®/Explicit. The following pseudo-code was used:

- from the current strain increment, update the total strain $\boldsymbol{\varepsilon}$ and the maximum strain $\boldsymbol{\varepsilon^{max}}$,
- using $f(\boldsymbol{\varepsilon})$, calculate the elastic strain:
  - if $\varepsilon_i \geq \varepsilon_i^{max}$: $\varepsilon_i^{el} = f(\varepsilon_i)$,
  - else $\varepsilon_i^{el} = \varepsilon_i - \varepsilon_i^{pl}$ where ε_i^{pl} is kept the same as in the previous increment,
- build the stiffness matrix $[\boldsymbol{C}]$ using E_1^0, E_1^1, E_2^0, E_2^1, G_{12}^0, G_{12}^1 and ν_{12},
- compute the Cauchy stress increment and update the total Cauchy stress.

For the sake of verification, the implemented subroutine was assigned to a single element of dimensions $1 \times 1 \times 1$ mm^3 and submitted to the loading history of the uniaxial and biaxial experiments. The stress-strain responses of the model were successfully compared to those of the experiments.

2.5. Validation

Previously acquired functional experimental data [2] were used to validate the constitutive models. The experimental set-up consisted of a 100 mm diameter hemispherical plunger loading a 250 mm diameter circular mesh through a 110 mm diameter circular patch, with fixation points represented by metal rods fitted with markers (more details available in [2]). The distribution of

reaction forces at the mesh fixation points was determined via rod continuum mechanics and the positions of markers were recorded by marker tracking system. An FE quarter model of this experiment was built in Abaqus®. This model featured 12553 M3D3 and M3D4 membrane elements and 340 B31 beam elements. The plunger and circular patch surfaces were modelled as frictionless analytical contact surfaces. Symmetry boundary conditions were imposed to the edges of the mesh, while the lower end of the rods were fixed. A vertical displacement was imposed to the plunger. The simulation was performed with the Abaqus®/Explicit solver. The numerical reaction forces at the fixation points were compared to three repeated experiments of a single cycle up to 310 N plunger force.

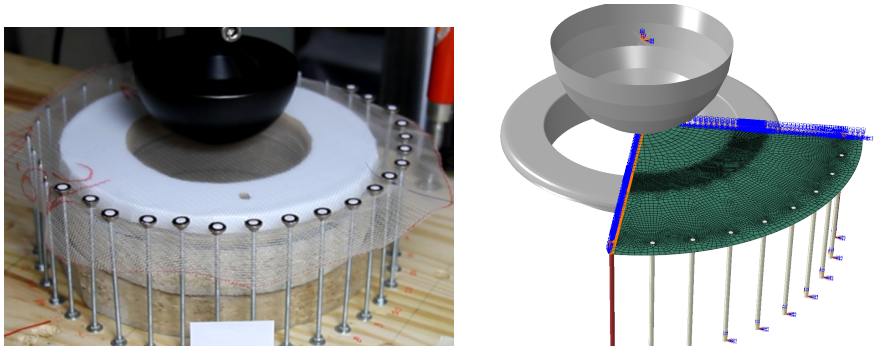

(a) Experimental setup (b) Corresponding FE model

Figure 3: Experimental setup of the plunger experiment allowing to measure fixation forces (a) and corresponding quarter FE model (b).

3. Results

3.1. Tensile test results

The response of the mesh subjected to tensile loading exhibited an anisotropic, non-linear behaviour (Figure 4). The warp direction is the stiffest, followed by the diagonal and weft directions. Under biaxial tension, the mesh appeared much stiffer, due to the strong coupling between the directions. The cyclic tests showed a permanent set after unloading, which increased when the maximum

applied strain increased (although it also slightly increased with the number of cycles, but to a minor extent). Note that further testing showed that this permanent set was not due to viscoelastic effects, as the residual strain was permanent and did not relax with time. A strong hysteresis was also observed during the unloading–reloading cycles.

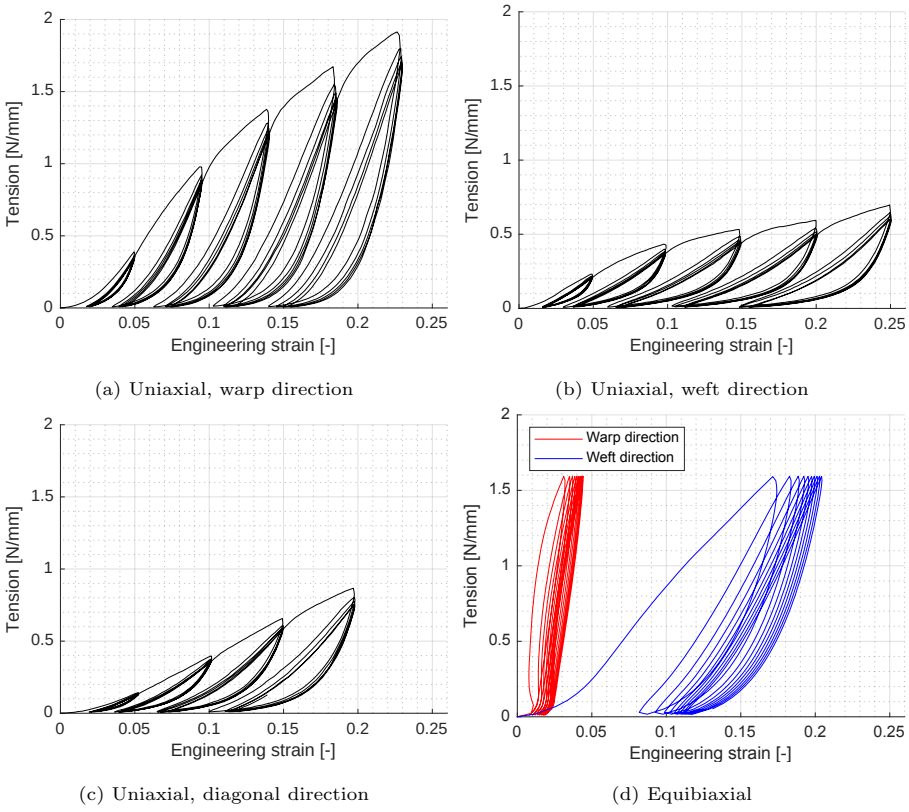

(a) Uniaxial, warp direction

(b) Uniaxial, weft direction

(c) Uniaxial, diagonal direction

(d) Equibiaxial

Figure 4: Experimental results obtained from cyclic tensile tests: tension vs nominal strain for uniaxial loading in warp (a), weft (b) and 45° diagonal (c) direction, and equibiaxial loading (d).

3.2. Model identification

The polynomial functions fitted to the response curves of the uniaxial tensile tests are shown in Figure 5a. They are in very good agreement with the 2$^{\text{nd}}$ order polynomial functions.

Regarding the yield evolution function, the ratio between the elastic strain and the total strain was the same in the weft and in the warp direction: $\frac{\dot{\varepsilon}_{11}^{el}}{\dot{\varepsilon}_{11}} = \frac{\dot{\varepsilon}_{22}^{el}}{\dot{\varepsilon}_{22}}$, confirming the isotropic nature of this phenomenon (Figure 5b).

All the identified material parameters are reported in Table 1.

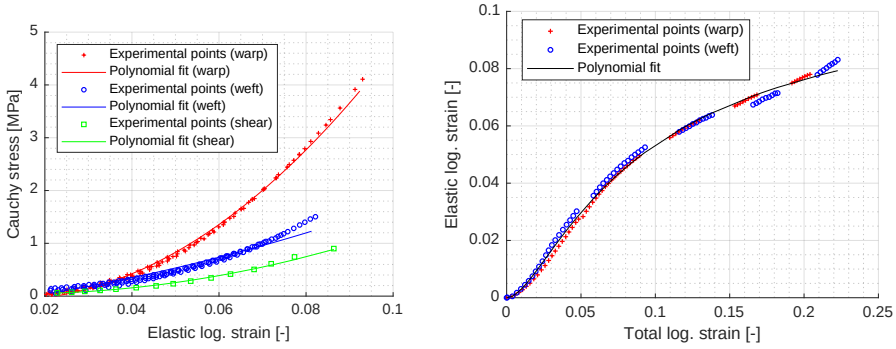

(a) Elastic behaviour

(b) Yield evolution function

Figure 5: Polynomial fits used to build the constitutive model: (a) polynomial functions used to derive 6 stiffness constants E_1^0, E_1^1, E_2^0, E_2^1, G_{12}^0 and G_{12}^1, in warp, weft and shear directions respectively; (b) polynomial function relating the part of elastic strain as a function of total strain: $\boldsymbol{\varepsilon}^{el} = f(\boldsymbol{\varepsilon})$.

Material parameter	Value	Unit
E_1^0	13.2	[MPa]
E_1^1	1205	[MPa]
E_2^0	13.3	[MPa]
E_2^1	187	[MPa]
G_{12}^0	0.87	[MPa]
G_{12}^1	148	[MPa]
ν_{12}	0.86	[-]
a	0.12	[-]
b	0.089	[-]
c	0.0027	[-]

Table 1: Identified material parameters for the hypo-elastoplastic constitutive model.

3.3. Model evaluation

The response curves predicted with a single finite-element to reproduce the uniaxial and biaxial cyclic tests are shown in Figure 6. As expected, the model captures the non-linearity, anisotropy and permanent set of the mesh behavior. Both uniaxial and biaxial responses are well reproduced. The unloading–reloading hysteresis is neglected, as a purely elastic behavior was assumed without viscous effects. The prediction of the model with respect to the experiments was quantified using the coefficient of determination (R^2). A satisfactory value of 0.94 was obtained for the overall data, despite hysteresis effects not reproduced by the model.

3.4. Validation results

Static equilibrium (defined as ratio of kinetic energy to external work lower than 1%) was reached with the FE model up to a 231 N force. Note that this is equivalent to a 182 mmHg intra-abdominal pressure, that is just above the mean pressure reported by Cobb et al. [5] for jumping in place (the most severe activity of his study). The strain field at this maximum force is shown in Figure 7a whereas the strain field after unloading is shown in Figure 7b. Strain concentrations are visible near the fixations, reaching values as high as 37%, which is out of the strain range covered in the experimental tests. The region under the plunger exhibits strains in the 10–20% range. After unloading, a residual strain field is present, which leads to a residual bulge as seen in Figure 7b.

Fixation forces were measured at an intermediate value of 60 N force, and were compared against their counterpart predicted by the FE model (Figure 8). A very good agreement can be noted, with a mean difference of 0.55 N. The numerical model successfully captured the heterogeneous force distribution, with higher forces along the warp direction.

Finally, the global force vs. displacement response curve in the plunger experiment was compared to the FE predictions (Figure 9). As previously mentioned, the FE model could satisfy mechanical equilibrium up to 231 N,

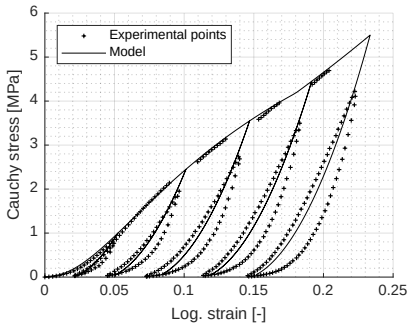

(a) Uniaxial, warp direction. $R^2 = 0.96$

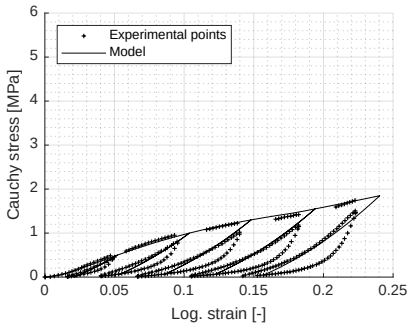

(b) Uniaxial, weft direction. $R^2 = 0.89$

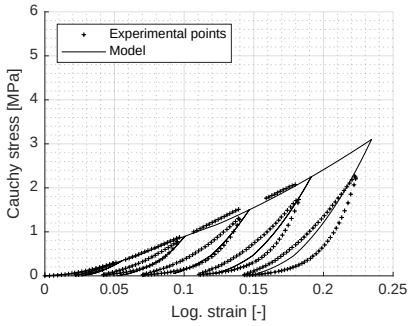

(c) Uniaxial, diagonal direction. $R^2 = 0.94$

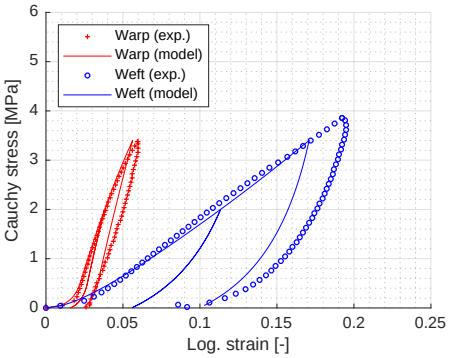

(d) Equibiaxial. $R^2 = 0.82; 0.74$ (warp; weft)

Figure 6: Identification of the constitutive model and comparison to experimental results in uniaxial tension (warp, weft and diagonal direction), and equibiaxial tension. The individual R^2 (coefficient of determination) are presented for each loading direction. The global R^2 of the model is 0.94. .

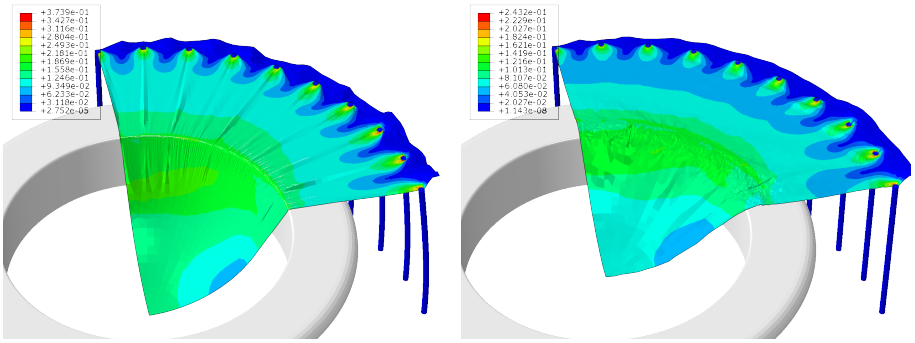

(a) At maximum (231 N) force (b) After unloading

Figure 7: Logarithmic membrane principal strain in the mesh at maximum loading (a) and after unloading (b), showing the residual strain and remaining bulge. Strain magnitudes are within the experimental domain of uni and biaxial tests, except in the close vicinity of fixation points.

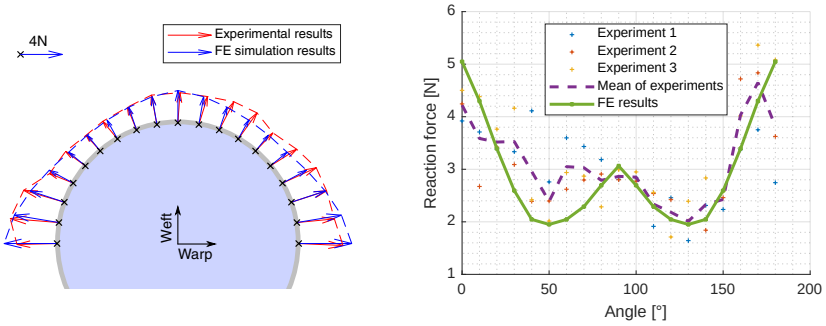

(a) Fixation force vectors (b) Force magnitude vs. angle

Figure 8: Experimental and numerical fixation forces at 60 N force: (a) force vectors at each fixation point and (b) force magnitude profile as a function of angle (0 and 180° corresponds to the warp direction and 90° to the weft direction.

and the curves can only be compared up to this point. A very good agreement between numerical and experimental results can be noted between 0 N and 140 N force ($R^2 = 0.97$). Beyond 140 N, the experimental curve starts to show a stiffer response. This is likely to be caused by regions of the mesh reaching strain values out of the range covered by experimental tests: in the model, stress was linearly interpolated outside the experimental domain whereas in reality, the non-linearity may induce a stiffer response. The remaining bulge after unloading (residual displacement at 0 force) is similar to experimental observations, showing the ability of the FE model to predict the permanent set even in such complex loading conditions.

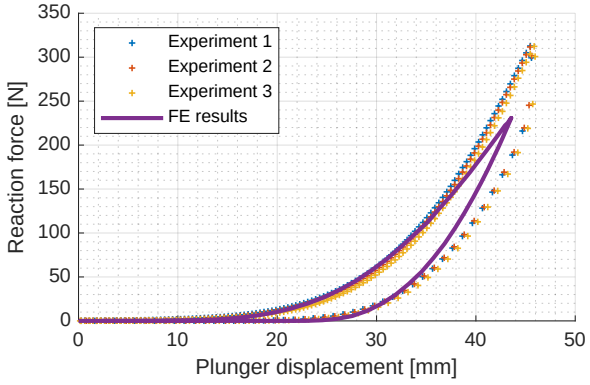

Figure 9: Global reaction force vs displacement of the plunger: comparison between experimental and finite element results. The coefficient of determination R^2 is 0.97.

4. Discussion

In this work, we have developed and validated an original constitutive model for knitted textiles which takes into account the major features needed to simulate numerically VIH interventions using these meshes: large deformations, non-linearity, anisotropy, and permanent set.

To our best knowledge, this is the first constitutive model of a knitted textile including all these features. Several homogeneous constitutive models of knitted

textile implants were previously proposed in simulations of abdominal hernia repair [13, 21, 29, 31]. They were based on anisotropic hyperelasticity and the material parameters were identified using uniaxial tensile tests. Effective porosity of the textile was previously taken into account [15]. Although the authors mention residual strains and corresponding experimental data in [21], their constitutive model did not account for permanent set.

Structural effects at the scale of pores were neglected in our continuum mechanics approach. The experiments used to fit material coefficients were done on small specimens with dimensions of about 10 pores (25 mm). It was shown that the continuum assumption is validated for predicting reaction forces at the fixation points. Although all our sample dimensions were designed to be at least 10 times larger than the unit cell size of the mesh (pores), scale effects may still exist and future work will also investigate the mechanical response of larger specimens. Another limitation of the identification procedure is the assumption of pure uni- and bi-axial stress and strain state in the center of the specimen, whereas full-field measurements could be employed in the future. However, as the plunger validation yielded satisfactory results, this limitation proved to have a limited impact.

Our model relies on exhaustive experimental data and may be particularly sensitive to the range of boundary conditions applied. In the current study, the range of stress ratios was limited to the two extremes (40:0 and 0:40 N ratios for uniaxial, 40:40 N for biaxial tests). When the material experiences stresses out of this range in FE simulations, the constitutive model extrapolates the response, which may deviate from the actual response. Accordingly, strain concentrations have to be considered with caution. However, the validation of the FE model through very good predictions of reaction forces at the fixation points in the plunger test shows that the domain of validity of our model remains wide enough to consider various applications. Note that the plunger force at which fixation forces have been extracted (60 N) is equivalent to a 47 mmHg intra-abdominal pressure, which is slightly above the range of pressures that have been reported for a Valsalva manoeuvre [5]. These moderate conditions

are consistent with what is expected for patients in hospital the first days or weeks after an abdominal wall repair surgery.

Note that fixation reaction forces were previously estimated using computational simulations for Dualmesh Gore® and DynaMesh® implants [19]. They were of the same order of magnitude compared to the present study. Present data are also comparable to data from porcine tissues despite strong dependence on mesh implant and fixation device [24].

A possible limitation of our membrane model is that the bending stiffness of the textile was neglected. Future work should characterize it using the Kawabata evaluation system [16] and consider it in the FE model as it may affect the prediction of creases, as shown in Figure 7. These creases may also occur during VIH surgical interventions and affect the biological integration process after surgery.

The main goal of our FE model is to be used in a simulation tool for assisting surgical interventions. A number of previous studies have highlighted the clinical significance of modeling the mechanical behavior of knitted textiles. Despite the different assumptions made in our model, it can still have clinical applications as for instance allowing the evaluation of permanent bulging and fixation forces post-surgery, before tissue integration and evolution of mesh properties. The model has been validated within a situation representing open defects, and is thus suited to evaluate techniques such as simple IPOM (Open Intraperitoneal Onlay Mesh) repair without primary closure of the defect.

Stiffness change of an implant as a consequence of cyclic loading experienced every day by a patient was quantitatively described with an attempt to simulate a preconditioned state of the mesh [28]. The authors observed stiffening induced by uniaxial cyclic load in DynaMesh®-IPOM implant. They remarked that the stiffening effect due to reload could possibly lead to higher fixation forces, fixation failure and hernia recurrence. In our work, stress softening was observed for a different textile implant under uniaxial cyclic load. While this might possibly lead to lower fixation forces, the permanent set data suggests possible functional issues related to the bulging. Once the implant is loaded to a certain

level, *e.g.* during coughing or exercise, it would remain permanently deformed creating a bulge in the abdominal wall. Further loading would even increase the bulge, with dramatic consequences.

Stiffening and permanent set effects after cyclic loading were also observed on mesh implants in air and at 37°C in physiological saline in four commonly used commercial hernia meshes [30]. Unlike frequent bench-top testing conditions (air, room temperature), body temperature and environment increase polymer chain mobility and facilitate the relative movement of the yarns. This leads to higher deformations for the same load and, by consequence, to a decrease in the overall stiffness. This behavior is modified as the abdominal wall tissues integrate biologically the implant.

As a macroscopic continuum, the proposed model does not aim at simulating and understanding yarn-scale phenomena. The mechanical behavior of the yarns (stretching and bending response), the frictional effects, as well as the knitting pattern and manufacturing process all contribute to the global behavior of the implant. This highlights the need for comprehensive yarn-scale models, which would be extremely valuable to understanding the relationship between yarn mechanics, mesh structure and global behavior. However, due to their high computational cost, they have been limited to simple patterns [10, 18, 20, 9]. Linking yarn-scale approaches to continuous models would be a major contribution to the development of meshes and simulation of their in-situ mechanical performance and possible failure mechanisms.

As the implant is loaded, the pores tighten until the yarns become locked. "Structural plasticity" may occur in this phase when the implant recovers its form only partially after unloading. Once the yarns are completely blocked, the material of the yarns takes over the structure and starts to deform under further load. Due to high complexity of the knitted patterns, both deformation mechanisms (structural and material) can coexist. Only some of the yarns can lock while the others can still move freely. Repetitive mechanical loading of the yarns can lead to alignment of polymer chains and increase the crystallinity, resulting in stiffening and possible local accumulation of damage and plastic

deformations. Our constitutive model pools together material and structural plasticity and effectively reproduces the observed permanent set. This unique asset makes the model suitable to assess effects of repeated loading such as implant bulging after surgical procedures and before the beginning of tissue integration process.

In addition to permanent set accumulation, mechanical fatigue of knitted textile implants for hernia repair is often neglected. It has been addressed in bench-top tests applying several hundreds or thousands of loading cycles [25, 26, 22]. However, hernia mesh fatigue testing raises many experimental challenges. Millions of loading cycles would be needed to simulate real life conditions. As polymers used to knit hernia mesh exhibit frequency-dependent mechanical behavior, the mechanical fatigue test should not be accelerated; it should be performed at some physiological frequency, e.g. that of the breathing or coughing. Such long-lasting characterization would ignore the process of tissue interaction and integration and provide information limited to the standalone implant. The material parameters of our model could possibly be modified to evolve with mechanical "ageing". However, the capacity of such constitutive model to take into account the accumulation of plastic deformation possibly leading to fatigue failure would strongly depend on the availability of relevant experimental data.

Although the constitutive behavior presented in this study has been developed for a specific mesh, it is representative of the general mechanical behavior of all meshes. By adjusting the model parameters and updating the evolution laws, it can reproduce mechanical features shared by all knitted meshes: nonlinearity, anisotropy, strong coupling and permanent [8]. Therefore, adjusting the model to other meshes should not raise major difficulties (just increasing polynomial order for instance) and should not require to develop additional mechanical tests.

5. Conclusion

Knitted textile implants are critical in many surgical procedures, as for instance hernia repair. For the first time ever, we have reported an extensive mechanical characterization of one of these biomaterials, including cyclic uniaxial tension, planar equibi-axial tension and plunger type testing. These tests showed the complex mechanical behavior with strong non linearity, anisotropy and permanent set. In addition, an anisotropic hypo-elasto-plastic constitutive modeling has been developed based on these experiments. Satisfactory identification and promising preliminary validation have been found.

In the future, combined characterization at fiber (micro), pore (meso) and implant (macro) scales should be performed to better understand the knitted textile mechanical behavior and strength. In particular, such experiments should enable to study separately the respective roles of the material and its structure. They should also lead to more advanced modeling of rupture.

Besides, implementation of this characterization and modeling approach to additional surgical knitted textiles, coupled with abdominal wall models, should enable to simulate abdominal wall repair biomechanics. Immediate post-op performance of repairs, varying surgical techniques and knitted textile implants, could then be assessed in terms of force at primary fixations (failure mode criterion) and residual bulging (patient satisfaction). The final objective would be to provide recommendations to clinicians.

Acknowledgements

The work was supported from European Regional Development Fund-Project "Application of Modern Technologies in Medicine and Industry" (No. CZ.02.1.01 /0.0/0.0/17_048/0007280).

References

[1] Ellen M. Arruda and Mary C. Boyce. A three-dimensional constitutive model for the large stretch behavior of rubber elastic materials. *J.*

Mech. Phys. Solids, 41(2):389–412, 1993. ISSN 00225096. doi: 10.1016/0022-5096(93)90013-6.

[2] Tristan Belzacq, Clément Ordrenneau, and Frédéric Turquier. Assessment of shear forces distribution at fixation points of textile based implants, 2018. US Patent 9,958,347.

[3] David C. Bosanquet, James Ansell, Tarig Abdelrahman, Julie Cornish, Rhiannon Harries, Amy Stimpson, Llion Davies, James C.D. Glasbey, Kathryn A. Frewer, Natasha C. Frewer, Daphne Russell, Ian Russell, and Jared Torkington. Systematic review and meta-regression of factors affecting midline Incisional hernia rates: Analysis of 14 618 Patients. *PLoS One*, 10(9):1–18, 2015. ISSN 19326203. doi: 10.1371/journal.pone.0138745.

[4] K. Cassar and A. Munro. Surgical treatment of incisional hernia. *Br. J. Surg.*, 2002. ISSN 00071323. doi: 10.1046/j.1365-2168.2002.02083.x.

[5] William S. Cobb, Justin M. Burns, Kent W. Kercher, Brent D. Matthews, H. James Norton, and B. Todd Heniford. Normal intraabdominal pressure in healthy adults. *J. Surg. Res.*, 129(2):231 – 235, 2005. ISSN 0022-4804. doi: https://doi.org/10.1016/j.jss.2005.06.015. URL http://www.sciencedirect.com/science/article/pii/S002248040500329X.

[6] A. Cordero, B. Hernández-Gascón, G. Pascual, J. M. Bellón, B. Calvo, and E. Peña. Biaxial Mechanical Evaluation of Absorbable and Nonabsorbable Synthetic Surgical Meshes Used for Hernia Repair: Physiological Loads Modify Anisotropy Response. *Ann. Biomed. Eng.*, 44(7):2181–2188, 2016. ISSN 15739686. doi: 10.1007/s10439-015-1503-4.

[7] Corey R. Deeken and Spencer P. Lake. Mechanical properties of the abdominal wall and biomaterials utilized for hernia repair. *J. Mech. Behav. Biomed. Mater.*, 2017. ISSN 18780180. doi: 10.1016/j.jmbbm.2017.05.008.

[8] Corey R. Deeken, Dominic M. Thompson, Ryan M. Castile, and Spencer P. Lake. Biaxial analysis of synthetic scaffolds for hernia repair demonstrates

variability in mechanical anisotropy, non-linearity and hysteresis. *J. Mech. Behav. Biomed. Mater.*, 2014. ISSN 18780180. doi: 10.1016/j.jmbbm.2014.06.001.

[9] T. D. Dinh, O. Weeger, S. Kaijima, and S. K. Yeung. Prediction of mechanical properties of knitted fabrics under tensile and shear loading: Mesoscale analysis using representative unit cells and its validation. *Composites Part B: Engineering*, 2018. ISSN 13598368. doi: 10.1016/j.compositesb.2018.04.052.

[10] M. Duhovic and D. Bhattacharyya. Simulating the deformation mechanisms of knitted fabric composites. *Composites Part A: Applied Science and Manufacturing*, 2006. ISSN 1359835X. doi: 10.1016/j.compositesa.2005.12.029.

[11] Savannah Est, Madeleine Roen, Tingying Chi, Adrian Simien, Ryan M. Castile, Dominic M. Thompson, Jeffrey A. Blatnik, Corey R. Deeken, and Spencer P. Lake. Multi-directional mechanical analysis of synthetic scaffolds for hernia repair. *J. Mech. Behav. Biomed. Mater.*, 2017. ISSN 18780180. doi: 10.1016/j.jmbbm.2017.02.009.

[12] JF Gillion, D Sanders, M Miserez, and F Muysoms. The economic burden of incisional ventral hernia repair: a multicentric cost analysis. *Hernia*, 20 (6):819–830, 2016.

[13] Belén Hernández-Gascón, Estefanía Peña, Jorge Grasa, Gemma Pascual, Juan M. Bellón, and Begonã Calvo. Mechanical response of the herniated human abdomen to the placement of different prostheses. *J. Biomech. Eng.*, 2013. ISSN 01480731. doi: 10.1115/1.4023703.

[14] Gerhard A. Holzapfel, Thomas C. Gasser, and Ray W. Ogden. A new constitutive framework for arterial wall mechanics and a comparative study of material models. *J. Elast.*, 2000. ISSN 03743535. doi: 10.1023/A:1010835316564.

[15] Andreas J. Horbach, Minh Tuan Duong, and Manfred Staat. Modelling of compressible and orthotropic surgical mesh implants based on optical deformation measurement. *J. Mech. Behav. Biomed. Mater.*, 2017. ISSN 18780180. doi: 10.1016/j.jmbbm.2017.06.012.

[16] Sueo Kawabata, Masako Niwa, and Yoshihiro Yamashita. A guide line for manufacturing "ideal fabrics". *International Journal of Clothing Science and Technology*, 1999. ISSN 17585953. doi: 10.1108/09556229910276296.

[17] U. Klinge, B. Klosterhalfen, J. Conze, W. Limberg, B. Obolenski, A. P. Öttinger, and V. Schumpelick. Modified mesh for hernia repair that is adapted to the physiology of the abdominal wall. *European Journal of Surgery*, 1998. ISSN 11024151. doi: 10.1080/11024159875000513 8.

[18] Dani Liu, Daniel Christe, Bahareh Shakibajahromi, Chelsea Knittel, Nestor Castaneda, David Breen, Genevieve Dion, and Antonios Kontsos. On the role of material architecture in the mechanical behavior of knitted textiles. *Int. J. Solids Struct.*, 2017. ISSN 00207683. doi: 10.1016/j.ijsolstr.2017.01.011.

[19] Izabela Lubowiecka. Behaviour of orthotropic surgical implant in hernia repair due to the material orientation and abdomen surface deformation. *Comput. Methods Biomech. Biomed. Engin.*, 18(3):223 – 232, 2015. doi: 10.1080/10255842.2013.789102.

[20] P. Justin McKee, Adam C. Sokolow, Jian H. Yu, Larry L. Long, and Eric D. Wetzel. Finite element simulation of ballistic impact on single jersey knit fabric. *Compos. Struct.*, 2017. ISSN 02638223. doi: 10.1016/j.compstruct.2016.11.086.

[21] Annie Morch, Laure Astruc, Jean François Witz, François Lesaffre, Pauline Lecomte-Grosbras, Damien Soulat, and Mathias Brieu. Modeling of anisotropic hyperelastic heterogeneous knitted fabric reinforced composites. *J. Mech. Phys. Solids*, 2019. ISSN 00225096. doi: 10.1016/j.jmps.2019.03.006.

[22] S Patterson, YC Ho, and WC Wang. The effect of cyclic loading on the mechanical performance of surgical mesh. In *EPJ Web of Conferences*, volume 6, page 21007. EDP Sciences, 2010.

[23] Margaret A Plymale, Ranjan Ragulojan, Daniel L Davenport, and J Scott Roth. Ventral and incisional hernia: the cost of comorbidities and complications. *Surgical endoscopy*, 31(1):341–351, 2017.

[24] Erwin Rieder, Martin Stoiber, Verena Scheikl, Marcus Poglitsch, Andrea Dal Borgo, Gerhard Prager, and Heinrich Schima. Mesh fixation in laparoscopic incisional hernia repair: Glue fixation provides attachment strength similar to absorbable tacks but differs substantially in different meshes. *J. Am. Coll. Surg.*, 212(1):80 – 86, 2011. doi: 10.1016/j.jamcollsurg.2010.08.015.

[25] Rita Rynkevic, Pedro Martins, Francisco Pereira, Nilza Ramião, and António A Fernandes. In vitro study of the mechanical performance of hernia mesh under cyclic loading. *Journal of Materials Science: Materials in Medicine*, 28(11):176, 2017.

[26] Sambit Sahoo, Katherine R DeLozier, Ahmet Erdemir, and Kathleen A Derwin. Clinically relevant mechanical testing of hernia graft constructs. *journal of the mechanical behavior of biomedical materials*, 41:177–188, 2015.

[27] Jason Smith and John D Parmely. Ventral hernia. In *StatPearls [Internet]*. StatPearls Publishing, 2019.

[28] A. Tomaszewska, I. Lubowiecka, and Szymczak C. Mechanics of mesh implanted into abdominal wall under repetitive load. Experimental and numerical study. *Journal of Biomedical Materials Research Part B*, 107(5): 1400 – 1409, 2019. doi: 10.1002/jbm.b.34232.

[29] A. Tomaszewska, D. Reznikov, C. Szymczak, and I. Lubowiecka. *Computer Methods, Imaging and Visualization in Biomechanics and Biomedi-*

cal Engineering. CMBBE 2019. Lecture Notes in Computational Vision and Biomechanics, chapter Constitutive Modelling of Knitted Abdominal Implants in Numerical Simulations of Repaired Hernia Mechanics. Springer, Cham, 2020. doi: 10.1007/978-3-030-43195-2_45.

[30] Shiny Velayudhan, Darren Martin, and Justin Cooper-White. Evaluation of dynamic creep properties of surgical mesh prostheses – uniaxial fatigue. *J. Biomed. Mater. Res. B Appl. Biomater.*, 91(1):287 – 296, 2009. doi: 10.1002/jbm.b.31401.

[31] Mark S. Yeoman, Daya Reddy, Hellmut C. Bowles, Deon Bezuidenhout, Peter Zilla, and Thomas Franz. A constitutive model for the warp-weft coupled non-linear behavior of knitted biomedical textiles. *Biomaterials*, 2010. ISSN 01429612. doi: 10.1016/j.biomaterials.2010.07.033.